Int J Adv Manuf Technol (2010) 47:1053–1063
DOI 10.1007/s00170-009-2227-0

ORIGINAL ARTICLE

Study on the rotary cup dressing of CBN grinding wheel and the grinding performance

Abdolhamid Azizi · Seyed Mehdi Rezaei · Abdolreza Rahimi

Received: 2 February 2009 / Accepted: 20 July 2009 / Published online: 6 August 2009

Abstract A systematic research is conducted to investigate the effect of rotary cup dressing on vitrified cubic boron nitride grinding performance in grinding of nickel-based superalloys. Grinding performance is evaluated mainly in terms of specific grinding energy and radial wheel wear. The number of active grits per unit area and their slope is considered as the two grinding wheel topographical key parameters for studying grinding performance. Cup dressing conditions with various speed ratios and overlap factors were investigated. In each case, the specific grinding energy and the radial wheel wear were experimentally measured, and then the effect of changing dressing parameters on the grinding performance is analyzed. To provide a view on how various parameters influence specific energy and the importance of wheel topography and grit workpiece interaction, a new specific grinding energy model is developed. Inputs to this model are workpiece parameters, grinding process parameters, and, in particular, the grinding wheel topographical parameters. This model is validated by experimental results. The theoretical values considering the complexity of the grinding process reasonably compare with the experimental results. The effect of number of active grits per unit area and their slope on specific grinding energy and then metal removal mechanism is investigated. The results revealed that the number of active grits per unit area has less effect on specific grinding energy than grits slope.

Keywords Cup dressing · Dressing forces · CBN · Grinding performance

Nomenclature

$2a$	Average distance between two successive CBN grits
a_d	Depth of dressing
a_n	Depth of cut
b_d	Dressing tool contact width
b_n	Grinding width
C	Concentration factor
D_g	Grinding wheel diameter
d_{CBN}	Mean diameter of CBN abrasive grits
d_{Dt}	Mean diameter of diamond grits
F_t	Tangential grinding force component
F_t'	Specific tangential grinding force (N/mm)
F_n'	Specific normal grinding force (N/mm)
f_n	Normal force on the grit (N)
H_b	Workpiece surface hardness
H_s	Workpiece bulk hardness
h	Grit depth of cut
h_{eq}	Equivalent chip thickness
i_d	Collision number
K	Wear coefficient of the workpiece (MPa^{-1})
k	Shear yield strength of the work
k_p	Shape parameter
L	Distance between adjacent tracks
l	Dimensionless distance between tracks
l_c	Length of arc of cut
l_{gd}	Geometrical contact length between dresser and grinding wheel
n_d	Dresser rotational speed rev/min

A. Azizi (✉)
Department of Mechanical Engineering,
Amirkabir University of Technology,
Tehran, Iran
e-mail: ha_azizi@aut.ac.ir

S. M. Rezaei · A. Rahimi
Department of Mechanical Engineering and New Technology Research Center, Amirkabir University of Technology,
Tehran, Iran

n_g	Number of active cutting points at contact
P	Grinding power
P_b	Probability of bond fracture
Q_w	Volumetric removal rate (mm^3/s)
q_d	Dressing speed ratio
q_g	Grinding speed ratio
U_d	Overlap factor
u	Specific grinding energy
V_a	Area grit density of the abrasive grits ($1/mm^2$)
V_g	Volumetric density of grits (concentration factor; $1/mm^3$)
v_d	Dresser surface speed
v_{fad}	Dresser horizontal feed
v_g	Grinding wheel surface speed
v_w	Workpiece speed
Δv	Relative speed between dresser and grinding wheel
W	Wear volume
α	Attack angle
β	Direction of the relative speed according to tangential
γ	Direction of the relative speed according to normal
λ_p	Scale parameter
μ	Coefficient of friction
μ_0	Friction factor at the interface between grit and workpiece

1 Introduction

The grinding operation is one of the most widely used operations for both metal removal and the production of precision components. The final surface topography generated on a grinding wheel is influenced and determined by the dressing conditions. The actual grinding wheel surface topography arises from the process of grit fracture and/or bond fracture during dressing process. Both the geometric and functional characteristics of the grinding wheel are therefore restored by the dressing process. The mechanic of the grinding process depends critically on the cutting edge density and their geometry. This affects grinding outputs as metal removal rate, wheel wear, and amount of consumed energy. Therefore, the wheel topography and the conditions under which it is prepared have a profound influence upon the grinding performance [1]. This is clearly evidenced by the grinding forces, power consumption, cutting zone temperatures, and the surface finish of the workpiece. Improved grinding performance should be obtainable through a more detailed understanding of the dresser–wheel and wheel–workpiece interactions.

Superalloys are a class of material broadly used in aerospace and power industries due to high performance at elevated temperatures [2]. High temperature strength and stability of superalloys which meet these criteria limit the machinability with traditionally cutting tool materials. Cubic boron nitride (CBN) grinding wheels may be a good alternative because of their high wear resistance and good thermal characteristic. The benefits of the hardness of CBN can only be achieved through simultaneously applying appropriate dressing method and dressing conditions [3]. Vitrified CBN grinding wheel is in wide acceptance due to the higher cost effectiveness of the entire grinding process. This is mainly due to longer wheel life, better surface finish, ease of preparation, and form holding [4]. Rotary tools are most suitable for vitrified CBN wheel truing and dressing [5]. They ensure high consistency of truing forces and wheel surface generation throughout the wheel life [4]. The life for rotary tools is also longer due to distribution of wear over many diamonds. It results in fewer interruptions to production process and consistency of truing and dressing operations. There are two types of rotary dresser configurations. In the first one, the axes of rotation of grinding wheel and rotary dresser are parallel (roll dresser). In the second case, the axes have perpendicular arrangement (cup dresser). For a parallel axes arrangement, arc of contact is short; hence, a smaller chance of collisions between diamond grits on dresser surface and CBN grits on grinding wheel surface exists. For perpendicular axes, the arc of contact is larger (approximately equal to width of the dresser). The dressing action is the result of collisions between abrasive grits of the wheel and diamond grits of the dresser. Few collisions produce a wheel with poor geometry and surface. Therefore, dressing with rotary cup is considered as a better dressing method than rotary roll dresser [4].

From material removal viewpoint, the most important statistical properties of the wheel surface topography are cutting edge parameters and their distribution. Cutting edge parameters are shape, height, density, and slope of grits [6, 7]. Active cutting edge density is the number of active cutting edges per unit area of the wheel surface. The active cutting edge density and their slope quantify the sharpness of the wheel [8].

In this paper, the experimental setup, which includes wheel dressing and surface grinding of Inconel 738, is presented first. The experimental grinding results including dressing and grinding forces, specific grinding energy, and radial wheel wear are compared and discussed. The dressing and grinding results are then analyzed. For better investigation of the grinding performance, development of a realistic model of the mechanic of the grinding process would be of great assistance. In this paper, along with some systematic experimental tests to study the grinding performance, a specific grinding energy model is proposed. The simulated specific energy is compared with the experimental results in order to evaluate the developed model.

2 Experimental work

Two series of dressing and grinding tests were conducted. In the first series, the effect of dressing parameters on dressing performance was investigated. The dressing parameters investigated are speed ratio, depth of dressing, and overlap factor.

The dressing system setup is illustrated in Fig. 1. It consists of a cup dresser rotated with an electric motor with speed control. The device is placed on the table of the grinding machine with feed control. The axis of the dresser spindle is perpendicular to the grinding wheel spindle axis. During dressing, the cup is traversed across the wheel width at a constant feed rate. Specification of the dresser and the grinding wheel is given in Table 1. For each set of experimental conditions, the dressing operations were repeated three times. The average value is used to minimize experimental errors. The dressing forces were measured by a Kistler dynamometer and then downloaded into a data acquisition system.

Following the grinding wheel conditioning, grinding tests were carried out in surface grinding mode. The variations in specific grinding energy and grinding wheel wear according to grinding and dressing inputs were measured. Grinding forces were measured via the dynamometer.

The method of grinding wheel wear measurement adopted was the "razor-blade" technique. After grinding the blade, the radial wear of the grinding wheel was measured using a profile projector.

To investigate the effect of dressing parameters on grinding wheel topography, replication technique along with Talysurf CCI instrument was used. After dressing, the topography of the wheel surface was recorded. Then, the record was analyzed to provide data for grit density and slope. For the medium porosity CBN grinding wheel (B91) which was used in this investigation, the grits with height more than 11 μm were considered as active grits [9]. The grit slope was obtained by differentiating the profile.

3 Results and discussions

3.1 Cup dressing system

During the dressing process, grinding wheel surface is generated by fracture of the grains at bond (bond fracture) and/or fracture within grains (grain fracture). Three rotary cup dressing parameters investigated in this study are depth of dressing (a_d), speed ratio (q_d), and overlap factor (U_d). For superabrasive wheels, the depth of dressing is usually very small, in the micrometer or submicrometer level. This is due to the high hardness of the abrasive. In cup dressing, the operation is carried out with low depth of dressing. This will cause grain fracture and bond fracture without pulling the grains out. The grinding wheel will have sharp grains and more open surface for chip flow [3]. Speed ratio is defined as the ratio of the dressing cup surface speed (v_d) divided by the grinding wheel surface speed (v_g). This is shown in Fig. 2a. q_d can be positive (unidirectional or down-dressing) or negative (counter-directional or up-dressing).

$$q_d = \pm \frac{v_d}{v_g} \tag{1}$$

The width of contact between the dressing cup and grinding wheel also influences dressing and grinding results. Overlap factor indicates the number of the contacts of a peripheral point of the grinding wheel with the active dressing wheel area. With respect to the dressing tool contact width (b_d) and the axial dressing feed $\left(\frac{v_{fad}}{n_d}\right)$, the overlap factor is defined as [10]:

$$U_d = b_d \frac{n_d}{v_{fad}} \tag{2}$$

where v_{fad} and n_d are dresser horizontal feed (in x direction) and dresser rotational speed, respectively. Thus, the number of collisions between CBN and diamond grits depends on the overlap factor.

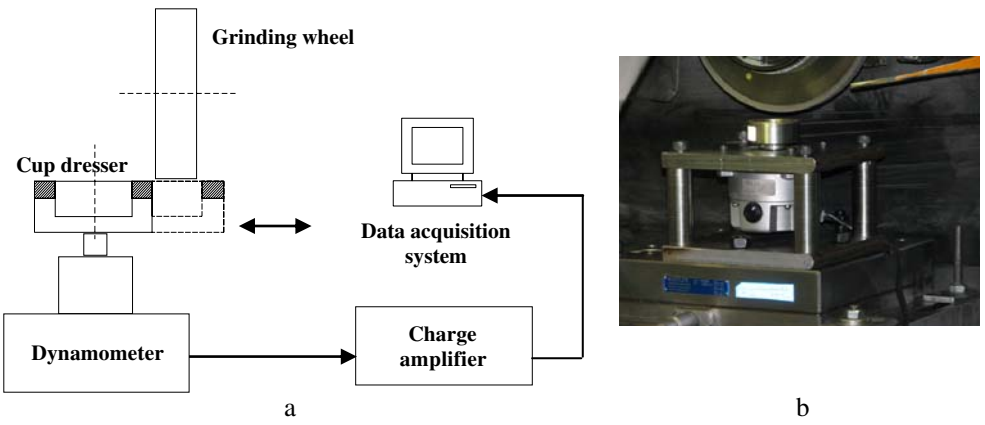

Fig. 1 Dressing system setup. **a** Schematic diagram of the dressing system. **b** Rotary cup dressing installation

Table 1 Summary of setup of parameters for the dressing and grinding system

Machine	
Model	Hauni-Blohm HFS 204
Max. spindle speed	4,000 rpm
Spindle power	10 kW
Grinding system	
Grinding wheel	1A1 200 10 3 51 B91 Vit. N V100
Wheel speed	20, 25, 30, 35, 40, 45, 50 m/s
Workpiece speed	48, 100, 180 mm/s
Depth of cut	0.01, 0.02, 0.03, 0.04, 0.05 mm
Workpiece	Inconel 738
Coolant	3% emulsion, 5.4 l/min
Dressing system	
Cup diameter	50 mm
Width of diamond rim	5 mm
Depth of diamond rim	3 mm
Dressing speed ratio	−0.6, −0.4, −0.2, +0.2, +0.4, +0.6, +0.8
Depth of dressing	0.003, 0.005, 0.007 mm
Overlap factor	50, 66, 100, 200
Cross-feed driver	Stepper motor

The direction of cutting speed of dresser and the wheel at the contact point "A" is shown in Fig. 2. Referring to Fig. 2b, relative speed Δv between rotary cup dresser and grinding wheel during dressing operation is equal to $\Delta v = v_d - v_g$.

During dressing process, the CBN grit on the grinding wheel interacts with different positions of the cup wheel. The induced force crushes the grit or fracture of the grit at bond is occurred. Fracture could be occurred in any direction which depends on the cracking orientation. Distribution of the grains on a grinding wheel and distribution of the cracks in a grain is random. Therefore, it is difficult to know the real orientation of the cracking in the dressing zone. It is assumed that the direction of the effective acted dressing force has the same direction as the relative speed [11].

3.2 Collision number of abrasive grits

During the dressing process, the removal of the wheel surface occurs due to the engagement of the diamond grits of the dressing tool with the CBN grits and the bonding matrix. The frequency of these collisions, their intensity, and the depth of the engagement of the diamond grits determine the condition of the surface of the grinding wheel. Therefore, the result of the dressing process such as dressing forces is governed and discussed by collision number. A mathematical model has been developed by Brinksmeier and Cinar [10] to determine the collision number between the diamond grits of a rotating dresser and the grits of a CBN grinding wheel. This model considers the kinematical influences of the dressing process and the specifications of both tools. The collision number takes into account the specifications of the CBN wheel and the diamond dressing tool, the overlap factor, and the speed ratio during dressing. Brinksmeier and Cinar have concluded that within each dressing stroke, a total collision number i_d occurs between CBN grit and the diamond grits is:

$$i_d = V_a l_{gd} (d_{CBN} + d_{Dt}) U_d |1 - q_d| \tag{3}$$

V_a is the area grit density of the abrasive grits and can be approximated to:

$$V_a = V_g^{\frac{2}{3}} \tag{4}$$

where V_g is the volumetric density of grits (concentration factor). d_{CBN} and d_{Dt} are the mean diameter of CBN abrasive grits and diamond grits, respectively. Also, l_{gd} is the geometrical contact length between dresser and grinding wheel which can be estimated to:

$$l_{gd} = \sqrt{D_g a_d} \tag{5}$$

D_g is the grinding wheel diameter.

Equation 3 shows a relation between the overlap factor, speed ratio, and the collision number. Not only the overlap factor but also the speed ratio has a linear influence on the

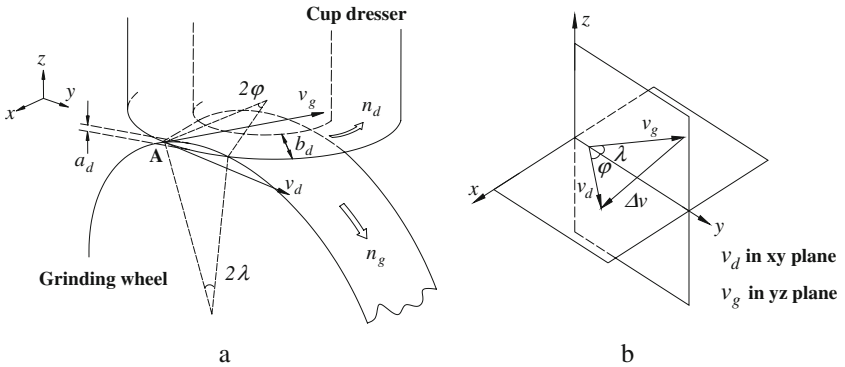

Fig. 2 Geometry of rotary cup dressing. **a** Cup dresser and the wheel at contact zone. **b** Relative speed at contact point

collision number and consequently on the dressing process. Based on Eq. 3, the influence of dressing parameters on collision frequency is shown in Fig. 3. As depicted in this figure, the linear influence of the speed ratio is not steady. It has a minimum at q_d=1 and i_d=0. This is the case if the grinding tool and the dressing tool rotate with the same speed and direction. In this case, both tools roll upon one another without any relative speed. The grinding abrasive grits are exposed to an increasing number of contacts with the diamond grits if a high value for i_d is selected.

3.3 Effect of dressing speed ratio on dressing forces

Figure 4 shows the variation of tangential and normal dressing forces against dressing speed ratio. The tangential dressing force decreases and the normal dressing force increases with raising speed ratio. This tendency was constant for various overlap factors. According to Fig. 3, decreasing speed ratio causes more collision frequency between diamond grits and CBN grits. The higher the collision number, the more CBN grits collide during dressing. Higher dressing forces are consequently expected.

Figure 5 shows the relative speed between rotary cup dresser and grinding wheel during dressing process at high and low speed ratio. Referring to Figs. 2 and 5, direction of the relative speed according to normal and tangential axis is γ and β, respectively. When speed ratio is small, the relative speed is large. Therefore, the tangential component of the relative speed is large but the normal component is low. As the resultant acted force has the same direction as the relative speed [11], tangential acted force on grits is high but the normal acted force is low. Therefore, collision takes place at the tangential direction to CBN grits and a shearing force acts on the grits. Then attritious wear and small crushing are produced on CBN grits. This will reduce the produced active cutting edges on grinding wheel surface after dressing with low speed ratio as shown experimentally in Fig. 6.

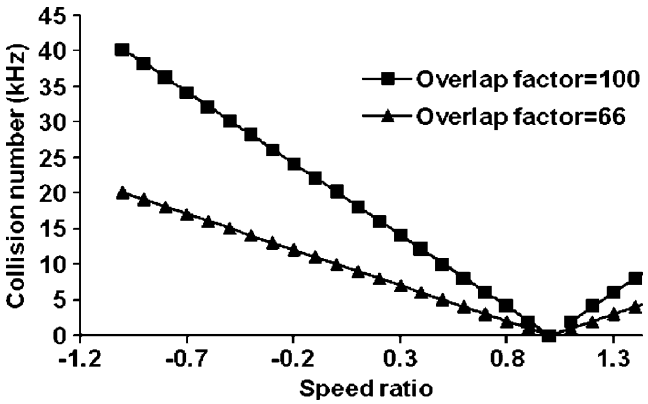

Fig. 3 Effect of dressing speed ratio and overlap factor on collision frequency

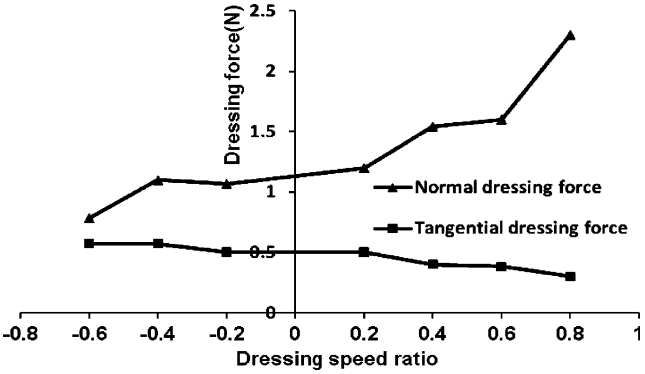

Fig. 4 Variation of tangential and normal dressing force with speed ratio

Under a higher speed ratio, harder radial contacts between dresser and grinding wheel occur which means that the active mechanism of dressing is shattering the grinding wheel surface layer. This is why the normal dressing force increases with an increase in speed ratio. This is in line with work done by Linke [12]. On the other hand, when speed ratio is over 0.8, the collision takes place at the radial direction of the CBN grits. Then, a compressive force acts on CBN grits and large scale crushing is produced on CBN grains. Consequently, the normal dressing force increases remarkably and sharp grain cutting edges are formed.

3.4 Effect of overlap factor on dressing forces

Figure 7 shows the variation of dressing forces against overlap factor. Assuming the feed and speed ratio remains constant, the dressing forces rise with increasing overlap factor. This is due to the generation of more number of collisions and contacts at a peripheral point of the grinding wheel with the active dressing cup. In addition, at higher overlap factor, the friction force between rotary cup dresser and grinding wheel will increase. These could be the reasons for the increase in dressing forces with rising overlap factor.

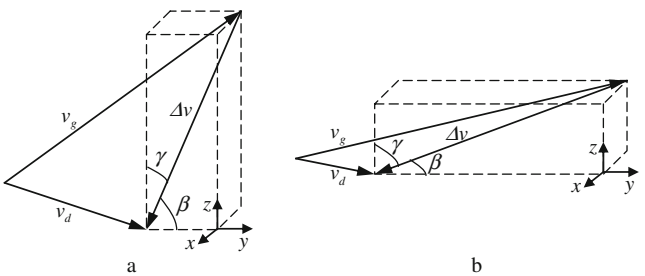

Fig. 5 Effect of speed ratio on relative speed and its horizontal, tangential, and normal components. **a** At high speed ratio. **b** At low speed ratio

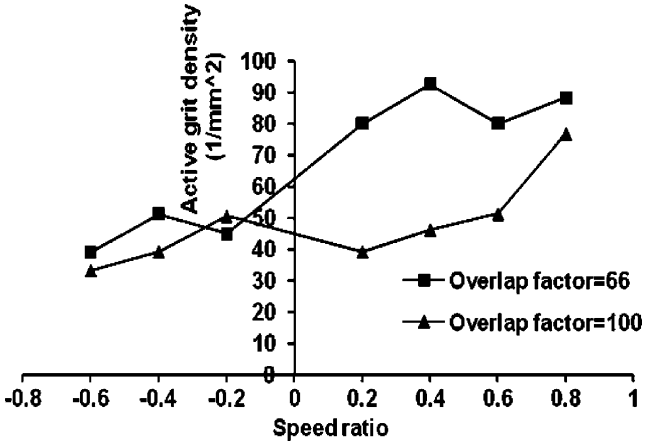

Fig. 6 Effect of speed ratio and overlap factor on active grit density on grinding wheel surface after dressing

3.5 Grinding performance

Grinding performance is mainly judged in terms of wheel wear and specific energy [13]. The grinding process is accompanied by wear of the abrasive wheel. The rate of this wear plays an important role in determining the efficiency of the grinding process and the quality of the workpiece.

Attritious wear causes smaller radial wear. But bond facture or grain pullout results in rapid usage of the grinding wheel. Grain fracture generates sharper cutting edges and is known as "self-sharpening" action of vitrified grinding wheels.

The grinding power P associated with the tangential force component F_t and wheel surface speed v_g in grinding operation can be written as [13]:

$$P = F_t v_g \tag{6}$$

The specific grinding energy is obtained from the following relationship [13]:

$$u = \frac{P}{Q_w} \tag{7}$$

Q_w is the volumetric removal rate given in terms of the grinding parameters as:

$$Q_w = a_n b_n v_w \tag{8}$$

where b_n is the grinding width, a_n is the depth of cut, and v_w is the workpiece speed.

Figure 8 shows the effect of varying dressing parameters on specific grinding energy. Decreasing speed ratio and increasing overlap factor causes an increase in the amount of specific grinding energy. This is because all generated wear flats on the grinding wheel surface are not removed during dressing and preparation of the grinding wheel. As mentioned, decreasing speed ratio or increasing overlap factor causes an increase in the amount of collision frequency. Large collision frequency means that grinding wheel surface topography is accompanied by grit microfracture. The grinding wheel surface goes flat and the number of active grits per unit area will decrease (as shown in Fig. 6). This results in a decrease in the active grits density. Hence, cutting points with larger flat area on grinding wheel surface are generated. Therefore, the grinding operation is carried out with higher energy consumption, but at the same time according to Fig. 9, smaller radial wheel wear is shown.

Figure 10 shows that larger radial wheel wear occurs when grinding tool is dressed at higher dressing speed ratio and lower overlap factor. Dressing with low speed ratio and high overlap factor causes many grit microfracture. The wear mechanism of the grinding wheel with microfractured grits on its surface is attritious wear which may cause smaller radial wear. The radial wear is attributed mainly to grain pullouts and the high wear rate is caused by the most protruding grains [14]. Pullout of these weakly held grains may be the cause of the radial wheel wear.

The relative amounts of grain and bond fracture during the grinding process also depend on the tangential acting force on grits on grinding wheel surface. With less bond fracture during the grinding process, less radial wheel wear

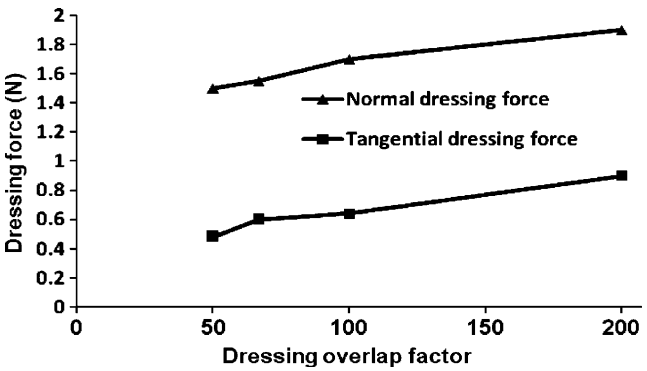

Fig. 7 Variation of tangential and normal dressing force with overlap factor

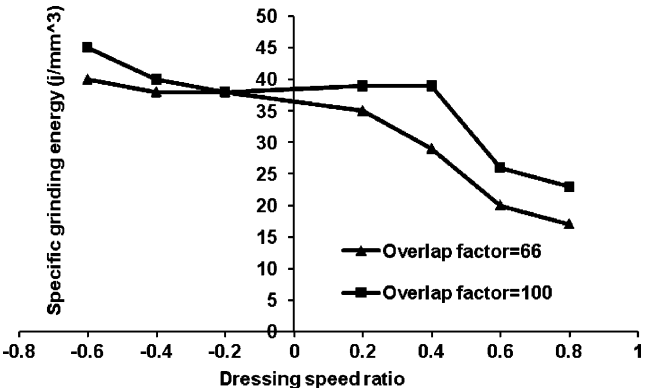

Fig. 8 Effect of varying dressing parameters on specific grinding energy

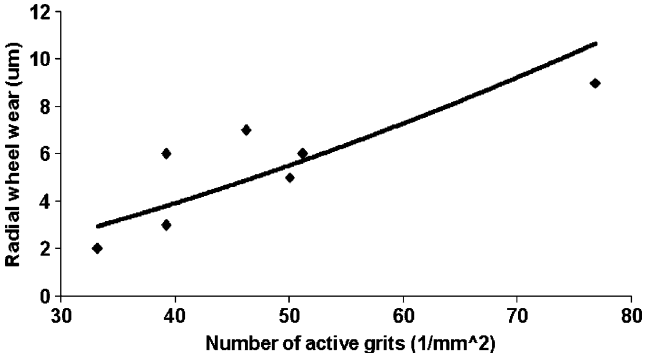

Fig. 9 Effect of the number of active grits on radial wheel wear

is expected. In practice, the overall wear of a grinding wheel can only proceed as fast as bond fracture occurs [13]. In order to determine the probability of bond fracture and thus grinding wheel loss, a statistical analysis was devised by Peklenik et al. [15]. A V-shaped tool that ploughs out a groove in the face of a grinding wheel was employed. Then, probability of bond fracture follows a Weibull distribution when the wheel is subjected to tangential force (F_t) on the abrasive grit. The cumulative distribution is given by:

$$P_b = 1 - \frac{1}{exp\left[\frac{F_t}{\lambda_p}\right]^{k_p}} \tag{9}$$

where k_p is the shape parameter. λ_p is the scale parameter and can be achieved by analyzing the given results. According to probability of bond fracture proposed by Peklenik et al., when the tangential force is applied to grits on the grinding wheel surface, the probability of bond fracture will be increased. Tangential force component induces predominantly tensile stress in bond. Therefore, the probability of bond fracture increases and radial wheel wear will be high. On the other hand, according to Eq. 6, increased tangential grinding force means higher amount of consumed energy during grinding operation. Therefore, the grinding process with more energy consumption will be accompanied by rapid radial wheel wear. This tendency is shown in Fig. 11 which was carried out in this investigation. It is clear that radial wheel wear increases with increasing specific grinding energy.

4 Specific grinding energy prediction model

One approach to investigate the grinding performance is to model the specific energy and relate it to wheel topography. The grinding specific energy model presented in this paper is based on a 3-D model for the interaction of a single hard pyramid-shaped grit in repeated sliding contact with workpiece surface. Therefore, the model is expanded for all of the active grits in grinding zone. Inputs to this model are the material properties of the workpiece, grinding operation parameters, and the grinding wheel topography parameters. In particular, the model indicates two key topographical parameters: the number of active grits per unit area and their slope. It means that via this model, the specific grinding energy is related to the grinding wheel surface parameters.

According to Eqs. 6 and 8, specific grinding energy can be written as:

$$u = \frac{F_t v_g}{a_n b_n v_w} \tag{10}$$

$\frac{F_t}{b_n}$ is the specific tangential grinding force and the quantity $\frac{a_n v_w}{v_g}$ is called the equivalent chip thickness (h_{eq}) [16]:

$$F_t' = \frac{F_t}{b_n} \tag{11}$$

$$h_{eq} = \frac{v_w a_n}{v_g} \tag{12}$$

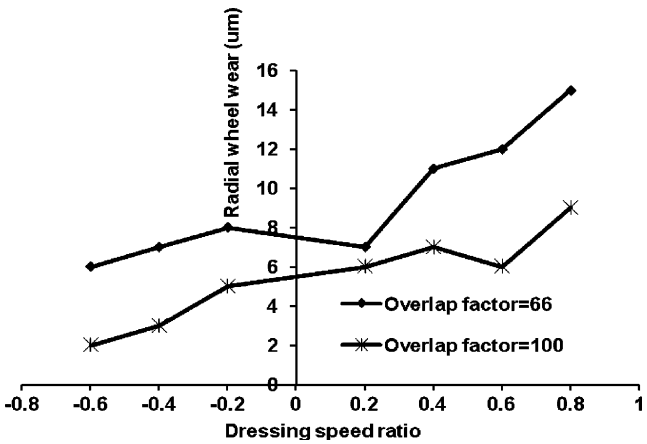

Fig. 10 Effect of varying dressing parameters on radial wheel wear

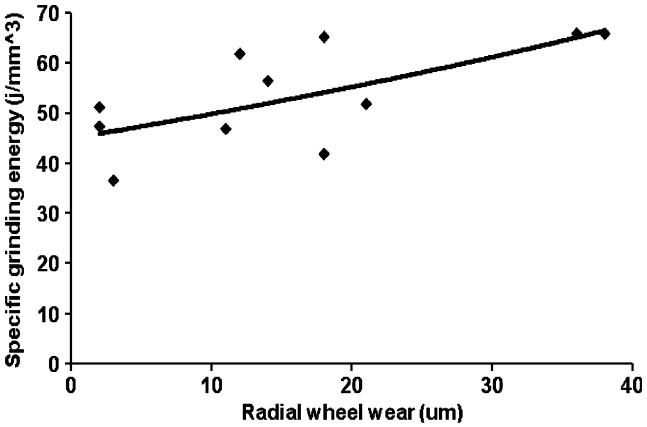

Fig. 11 Specific grinding energy against radial wheel wear

Therefore, specific grinding energy can be rewritten as:

$$u = \frac{F_t'}{h_{eq}} \tag{13}$$

The 3-D abrasion model used to predict grinding forces and then specific grinding energy as a function of grinding wheel topography uses the pyramid-shaped grit as shown in the Fig. 12 [8].

Using this approach, the grits of a grinding wheel can be represented as hard pyramids. Hence, the forces on a single grit and the specific grinding energy can be calculated from the workpiece material properties, the grinding wheel surface parameters, and the grinding process parameters.

For a given attack angle of abrasive grit, α, and friction factor at the interface between grit and workpiece, μ_0, the regime of contact (rubbing, plowing, or cutting) can be determined. For each regime, the horizontal force, the wear coefficient of the workpiece (K), and the coefficient of friction (μ) can be calculated. They are related to friction factor (μ_0), the ratio of bulk to surface hardness of the workpiece $\left(\frac{H_b}{H_s}\right)$, and the dimensionless distance between tracks (l). The equations for μ and K and the criteria for which contact regime is present are reported in sliding a hard rough surface against a soft surface [17–19].

$$\mu = \left(\frac{2}{\pi}\right)^{0.5} \frac{tan\alpha}{l^{0.25}} \left(1 - \mu_0 \left[1 + \frac{\pi}{4tan^2\alpha}\right]^{0.5}\right) \tag{14}$$

$$K = 0.003 \frac{tan^3\alpha}{\mu_0 k l^{0.5}} \sqrt{\frac{H_b}{H_s}} \tag{15}$$

Using this approach and the definition of K [19]:

$$K = \frac{W}{f_n L} \tag{16}$$

f_n is normal force on the single grit and L is the distance between adjacent tracks. W is the wear volume for single grit [19]:

$$W = \frac{h_{eq} L l_c}{n_g} \tag{17}$$

where l_c is the length of arc of cut and η_g is the number of cutting points at contact.

Thus, specific normal force can be written as:

$$F_n' = \frac{n_g f_n}{l_c} = \frac{h_{eq}}{K} \tag{18}$$

and noting that specific tangential grinding force

$$F_t' = \mu F_n' \tag{19}$$

then

$$F_t' = \mu \frac{h_{eq}}{K} \tag{20}$$

The specific grinding energy is given by inserting Eq. 20 into Eq. 13:

$$u = \frac{\mu}{K} \tag{21}$$

By combining Eqs. 14, 15, and 21:

$$u = 266 \frac{\mu_0 k l^{0.25}}{tan^2\alpha \sqrt{\frac{H_b}{H_s}}} \left\{1 - \mu_0 \left(1 + \frac{\pi}{4tan^2\alpha}\right)^{0.5}\right\} \tag{22}$$

It is still necessary to define the dimensionless distance between tracks (l), for calculation of specific energy. l is relative overlap (overlap/scratch width) of successive grinding scratch [18]. According to Fig. 13, this is given as:

$$l = \frac{L}{htan\alpha} \tag{23}$$

The distance between adjacent tracks created by two successive active points is approximated by Eq. 24. This

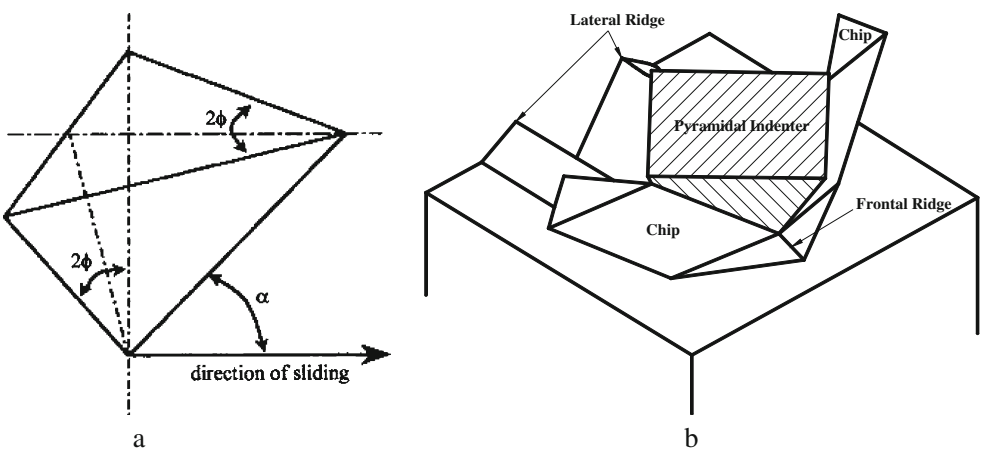

Fig. 12 **a** 3-D abrasive grit model. **b** Simultaneous cutting and plowing by an abrasive grit [8]

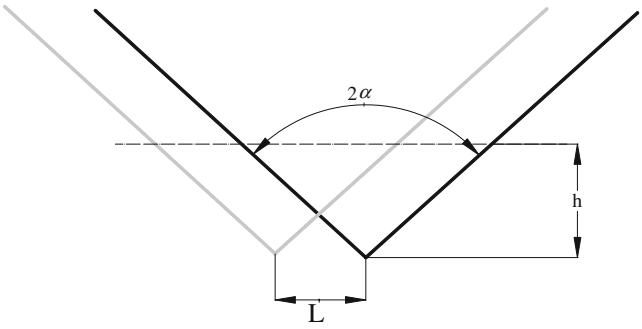

Fig. 13 Distance between adjacent tracks created by two successive active points

is in accordance with the number of active cutting points at contact calculated.

$$L = \frac{l_c}{n_g} \tag{24}$$

$\frac{n_g}{l_c}$ is the linear density of active grits per unit length and from wheel-work kinematics [13]:

$$l_c = \sqrt{D_g a_n} \tag{25}$$

where α_n is depth of grinding process.

h is grit depth of cut and from the wheel-work relations is further computed using the following equation [13]:

$$h = 2aq_g\sqrt{\frac{a_n}{D_g}} \tag{26}$$

q_g is the grinding speed ratio between grinding wheel surface speed and workpiece speed. $2a$ is the average distance between two successive CBN grits on grinding wheel surface [20]:

$$2a = \left(\frac{0.74\pi}{C}\right)^{1/3} d_{CBN} \tag{27}$$

where C is concentration factor, which indicates the amount of abrasives contained in the grinding wheel. This means that $2a$ depends on the characteristic grain size d_{CBN} and the concentration factor.

According to the last two equations and the grinding wheel used, the grit depth of cut is given by:

$$h = 2.1 d_{CBN} q_g \sqrt{\frac{a_n}{D_g}} \tag{28}$$

Thus,

$$l = \frac{D_g tan\alpha}{2.1 d_{CBN} q_g n_g} \tag{29}$$

Using Eqs. 22 and 29, specific grinding energy from the presented model is

$$u = 266\frac{\mu_0 k\left(\frac{D_g tan\alpha}{2.1 d_{CBN} q_g n_g}\right)^{0.25}}{tan^2\alpha\sqrt{\frac{H_b}{H_s}}}\left\{1 - \mu_0\left(1 + \frac{\pi}{4tan^2\alpha}\right)^{0.5}\right\} \tag{30}$$

According to Eq. 30, specific grinding energy is effected by:

– Workpiece parameters, such as shear yield strength of the work surface k, the microhardness of the work surface, the bulk hardness of the workpiece (in this

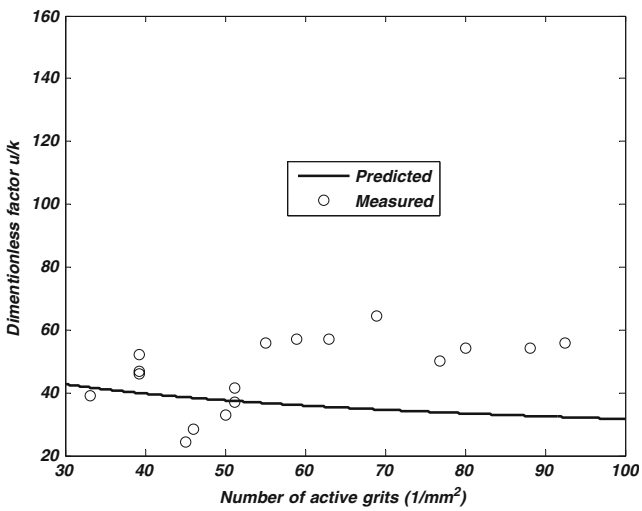

Fig. 14 Effect of active grits on specific grinding energy

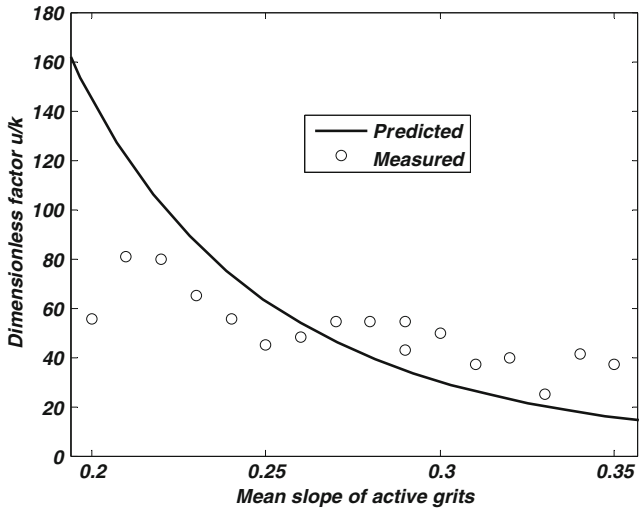

Fig. 15 Effect of active grits sharpness on specific grinding energy

study, for simplicity, the value of $\sqrt{\frac{H_b}{H_s}}$ is approximated to be close to unity), and the coefficient of the friction
- Machining parameters, such as the speed ratio between grinding wheel surface speed and workpiece speed and grinding depth of cut
- The grinding wheel topography parameters, number of active grits at contact (n_g), and slope of the active grits (tan a)

The validity of the presented model is verified through a comparison between the predicted and measured values of the specific energy within a range of active grits and their slope. Variation of two key parameters on specific grinding energy from the model and experimental results is shown in Figs. 14 and 15. It can be clearly seen that the results of the proposed model have the same trend with those experimentally obtained. In general, specific grinding energy is found to decrease as the number of cutting points and their slope increase.

The inverse relationship between specific energy and grinding wheel surface parameters is often referred to as the "size effect" [21, 22]. Such large specific energies in grinding would indicate that the energy expenditure is mainly associated with ductile flow (plowing). Actually material removal takes place by the cutting action. Furthermore, the specific energy increases as the number of cutting points and their sharpness decrease. This is due to an increased tendency for ductile flow rather than cutting as the abrasive grits interact with the workpiece. Grinding with sharp grits causes an increase in the cutting action and there is no wasted energy due to plowing.

It can be seen that the rate of decrease of specific energy against slope of active grits is higher than that against number of active grits. This means that changing the cutting point's sharpness has a more powerful effect on specific grinding energy. To have sharp grits, dressing with high speed ratio and low overlap factor is required. According to cup dressing experimental results presented, dressing with speed ratio greater than +0.2 is recommended.

For selected operational parameters in this investigation, the variation of slope through 0.2 to 0.25 has greater effect on specific grinding energy than through 0.3 to 0.35. This may account for changing metal removal mechanism from plowing to cutting action.

5 Conclusions

An attempt was made to elucidate how the grinding wheel surface can affect the grinding performance. This aim was achieved by a series of systematic experiments along with presenting a new specific grinding energy model. The radial wheel wear and specific grinding energy were considered as indicators for evaluation of grinding performance. From this study, the following conclusions can be drawn:

- Contact kinematics in rotary cup dresser is responsible for generation of an appropriate grinding wheel surface.
- The radial wheel wear is due to vitrified bond fracture and abrasive grits pull out. Increasing the tangential acting force on CBN grits result in an increase in the radial wheel wear. It is clear now that increasing the cutting points on grinding wheel surface causes a drop in the amount of consumed energy but at the same time larger radial wheel wear is expected. This is due to more grains pull out as the prevailing wear mechanism.
- The theoretical relation between specific grinding energy and number of cutting points and their slope as the grinding wheel topography indicators has been presented. The specific energy obtained from the model has been compared with those experimentally observed. A reasonable agreement between the modeled and experimental values is achieved. Results reveal that specific energy inversely decreases when number of cutting points and their slope increase. Specific energy diminishes progressively regardless of whether number of cutting points or their slope is further increased. This can be attributed to an increased tendency for cutting action and chip formation rather than plowing and sliding as the abrasive grains interact with the workpiece.
- The slope of cutting points has greater effect on specific grinding energy than the number of active cutting points.

Acknowledgments Authors wish to thank Dr. A. Abdullah for his valuable help in the experimental program. The assistance given by the staff of the Machining Research Laboratory of Mechanical Engineering Department of Amirkabir University of Technology is also acknowledged.

References

1. Huang H (2001) Effects of truing/dressing intensity on truing/dressing efficiency and grinding performance of vitrified diamond wheels. J Mater Process Technol 117:9–14
2. Qiang L, Xun C, Nabil G (2007) Assessment of $Al_2O_3$and superabrasive wheels in nickel-based alloy grinding. Int J Adv Manuf Technol 33:940–951
3. Chen X, Rowe WB, Cai R (2002) Precision grinding using CBN wheels. Int. J. Mach. Tools Manuf 42:585–593
4. Prusak Z, Webster JA, Marinescu ID (1997) Influence of dressing parameters on grinding performance of CBN/seeded gel hybrid wheels in cylindrical grinding. Int. J. Prod. Res 35: 2899–2915
5. Klocke F, Konig W (1995) Appropriate conditioning strategies increase the performance capabilities of vitrified-bond CBN grinding wheels. Annals of the ClRP 44:305–310
6. Baseri H, Rezaei SM, Rahimi A, Saadat M (2008) Analysis of the disc dressing effects on grinding performance—part 1: simulation of the disc dressed wheel surface. Mach. Sci. Technol 12(2):183–196

7. Baseri H, Rezaei SM, Rahimi A, Saadat M (2008) Analysis of the disc dressing effects on grinding performance—part 2: effects of the wheel topographical parameters on the specific energy and workpiece surface roughness. Mach. Sci. Technol 12(2):197–213
8. Badger JA, Torrance AA (2000) A comparison of two models to predict grinding forces from wheel surface topography. Int. J. Mach. Tools Manuf. 40:1099–1120
9. Cai R, Rowe WB (2004) Assessment of CBN wheels for precision grinding. Int. J. Mach. Tools Manuf. 44:1391–1402
10. Brinksmeier E, Cinar M (1995) Characterization of dressing processes by determination of the collision number of the abrasive grits. Annals of the ClRP 44(1):299–304
11. Baseri H, Rezaei SM, Rahimi A, Rezaeian M (2007) Modeling of disc dressing forces. Mach. Sci. Technol 11(2):201–216
12. Linke B (2008) Dressing process for vitrified bonded grinding wheels. Annals of the CIRP 57:345–348
13. Malkin S (1989) Grinding technology, theory and applications of machining with abrasives. Ellis Horwood, Chichester
14. Shi Z, Malkin S (2006) Wear of electroplated CBN grinding wheels. Trans ASME J Manuf Sci Eng 128:110–118
15. Peklenik J, Lane R, Shaw MC (1964) Comparison of static and dynamic hardness of grinding wheel. Trans ASME J. Eng. Indust 86:294–298
16. Peters J (1984) Contribution of CARP research to industrial problem in grinding. Annals of the CIRP 33:193–197
17. Williams JA, Xie Y (1992) The generation of wear surfaces by the interaction of parallel grooves. Wear 155:363–379
18. Xie Y, Williams JA (1993) The generation of worn surfaces by the repeated interaction of parallel grooves. Wear 164:864–887
19. Xie Y, Williams JA (1996) The prediction of friction and wear when a soft surface slides against a harder rough surface. Wear 196:21–34
20. Dabrowski L, Marciniak M (2004) Investigation into phenomenological aspects of the grinding process. Proc Inst Mech Eng B J Manuf Eng 218(5):495–503
21. Hwang TW, Evans CJ, Malkin S (1999) Size effect for specific energy in grinding of silicon nitride. Wear 225:862–867
22. Hwang TW, Malkin S (1999) Upper bound analysis for specific energy in grinding of ceramics. Wear 231:161–171